
# New catalysts for green BTX

## Zeolite catalysts for 2,5-dimethylfuran to benzene, toluene and xylene

Master's thesis in materials chemistry

OSCAR HELLGREN

DEPARTMENT OF CATALYSIS
CHALMERS UNIVERSITY OF TECHNOLOGY
Gothenburg, Sweden 2023
www.chalmers.se

Master's thesis 2023

# New catalysts for green BTX

OSCAR HELLGREN


CHALMERS
UNIVERSITY OF TECHNOLOGY

Department of chemistry and chemical engineering
*Kompetenscenter för Katalys*
Per-Anders Carlsson group
Chalmers University of Technology
Gothenburg, Sweden 2023

New catalysts for green BTX
Zeolite catalysts for 2,5-dimethylfuran to benzene, toluene and xylene
Oscar Hellgren



Supervisor: Guido de Reijer, Applied chemistry
Examiner: Per-Anders Carlsson, Kompetenscenter för katalys

Master's Thesis 2023
Department of Chemical Engineering
Division of Applied Chemistry
Per-Anders Group
Chalmers University of Technology
SE-412 96 Gothenburg
Telephone +46 31 772 1000

Typeset in LaTeX
Gothenburg, Sweden 2023

# Abstract

This thesis examines the impact of aluminium and gallium content in faujasite and mordenite zeolites on the conversion and selectivity of 2,5-dimethylfuran into benzene, toluene and xylene. An optimum aluminium content for faujasite was confirmed, and lies around a silicon to aluminium-ratio of 6.05. Gallium introduced by wet impregnation was shown to improve conversion and selectivity for faujasites with high aluminium content, and for mordenite. Gallium treated mordenite was found to have the highest selectivity and conversion out of all examined zeolites.

# Acknowledgements

I would like to extend my deepest thanks to my supervisor Guido de Reijer, your tireless support and guiding hand has made this thesis possible. Thank you for the cheers when the going got tough.

I want to thank my examiner Per-Anders Carlsson and everyone in his research group for taking me on and letting me be a part of their team for the past months.

Thanks to Magnus Gustaver for an excellent Overleaf template

Tack Linn, för stödet.

Oscar Hellgren, Gothenburg, 2023

# List of Acronyms

Below is the list of acronyms that have been used throughout this thesis listed in alphabetical order:

| | |
|---|---|
| BET | Brunauer Emett Teller |
| BTX | Benzene, toluene and xylenes |
| EFAl | Extraframework Aluminium |
| FAU | Faujasite |
| FCC | Fluid catalytic cracking |
| MFC | Mass flow controller |
| MOR | Mordenite |
| TPD | Temperature programmed desorption |
| USY | Ultrastable zeolite Y |
| XRD | X-ray diffraction |
| XRF | X-ray fluorescence |

# Contents

# List of Figures

# List of Tables

# 1
# Introduction

In 2021, benzene, toluene and xylenes [BTX] accounted for 28% of global petrochemical consumption [7]. Still, the BTX market is growing and the global demand for BTX is predicted to increase in the coming years [8]. In fact, the possibility of environmentally sustainable BTX and a growing public consciousness of the environment is predicted to be one of the factors for increased global demand for BTX.

BTX production is however not environmentally sustainable at this time. Historically, the production of benzene, toluene and xylene has been exclusively based on fossil fuels. Since the 1950's, the process has been based on coal tar and later naphtha as a starting material [9]. Today, BTX production is still dominated by catalytic reforming or steam cracking of naphtha [10]

The main use of BTX in industry is as components in plastics production; benzene is used to produce polystyrene and nylon-6, toluene in the production of polyurethane and xylene in the production of polyethylene terephthalate. BTX, therefore, is tied to the world demand for plastic packaging and the global annual production can be measured in billions of tons. Finding an environmentally sustainable way of producing these commodities from renewable materials is an alluring prospect.

Previous studies have shown that one way of producing BTX from 2,5-dimethylfuran via zeolite catalysis is possible [11]. Dimethylfuran can be produced from cellulose from forestry and agricultural waste, making it a sustainable alternative to what is generally done today [12]. The choice of catalyst is crucial in making this reaction more optimized. Zeolites exist in many structures and vary in atomic content, posing the question of how these parameters may be influenced to tailor the catalyst for green BTX production.

This thesis aims to examine the conversion of 2,5-dimethylfuran over solid zeolite catalysts of Faujasite and Mordenite structures, and how these catalysts influence the reaction selectivity into benzene, toluene and xylenes. Post-synthesis methods of maximizing conversion and selectivity of BTX with variations in aluminium and gallium content will also be studied.

# 2

# Theory

## 2.1 Heterogeneous catalysis

Heterogeneous catalysis effectively works in four steps:

1. Adsorption
2. Dissociation
3. Reaction
4. Desorption

All of these steps have activation energies of their own, but the sum of the energies is lower than that of the uncatalysed reaction. This whole process proceeds without consuming the catalyst, as per the definition of catalysis.

Homogeneous catalysis, where catalyst and reactants exist in the same, often fluid, phase has one major advantage. The fluids are dispersed within each other on a molecular level, maximizing the available area for catalyst to interact with reactants. The main drawback of homogeneous catalysis is the separation of species after reaction, as separation processes are energy intensive. If solvents are used for homogenization, further separation demands are posed for solvent extraction.

Heterogeneous catalysis is superior in terms of separation. The more important factor is the extent of solid/fluid phase interaction, most often how much solid surface area is available with active catalytic sites. A solid catalyst likely requires a high specific surface area to be at all effective. This is where zeolites excel. Their regular microporous frameworks constitute vast areas per gram, making them competitive in reactivity while negating the main drawback of homogeneous catalysis. One additional aspect of microporous catalysts is their shape selectivity, as molecules have a limited free space within the pore network. A zeolite can be selected for a specific reaction, with a pore structure that favours molecules the size of the specified product.

Heterogeneous catalysis does however encounter one important drawback, namely catalyst deactivation. For the intents of this thesis the most significant mode of catalyst deactivation is fouling by carbon species deposition. As reaction proceeds over the solid surface it sometimes proceeds too far, creating bulky hydrocarbon species, called coke, over the active site. These species do not dissociate from the surface, instead remaining and blocking the sites' potential for further catalysis. In time, the catalyst will be completely spent and inactive, requiring regeneration. This is usually done by heating the catalyst in an oxidative atmosphere, gasifying the coke

species to free up the sites. Most of the activity is restored to the catalyst but some loss may be irreversible due to poisoning, thermal degradation, chemical attrition etc.

## 2.2 Zeolites

A zeolite is a microporous aluminosilicate with a framework of silicon, oxygen, and aluminium, where the silicon and aluminium are tetrahedrally coordinated to oxygen. As each oxygen binds to two tetrahedral structures each, the tetrahedra are arranged in rings of various sizes, as in figure 2.1. These rings conform together in various ways to form large networks of silicon, aluminium and oxygen, implementing voids in a regular porous structure. Pore size varies with framework type, and frameworks with large enough pores allow for larger molecules to permeate the framework.

Each tetrahedrally coordinated silicon atom is charge neutral, while tetrahedrally coordinated aluminium carries a negative charge, stabilized by an extra-framework cation. A further requirement for the framework is the so called Löwensteins rule, stating that Al-O-Al linkages are most often avoided [13].

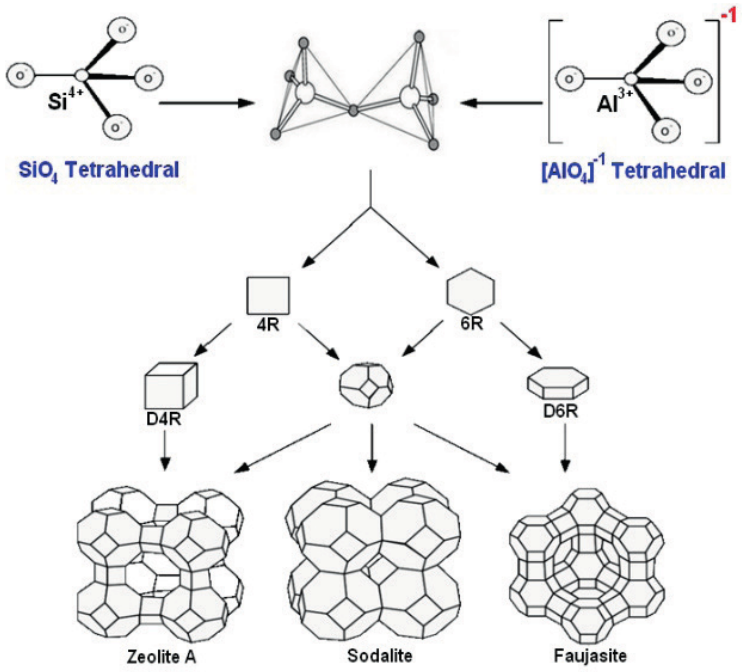


**Figure 2.1:** Zeolite formation from the tetrahedrals [1]

The charge imbalance created by framework aluminium carries with it an implication on the structural stability of the framework. The cation required for charge compensation will acquire kinetic energy as temperature increases and it will eventually escape the framework, making the aluminium tetrahedra unstable. Higher aluminium content leads to a higher amount of unstable tetrahedra, implying a lower thermal stability as zeolite aluminium content increases [14].

There are many ways for the aluminosilicate framework to be arranged, and aluminium content, paired with different cations and templating agents, can induce specific frameworks with further variation in pore structure. Additionally, the charge imbalance of framework aluminium is crucial due to its role in acid catalysis. If the counter-ion for the negatively charged alumina species is a proton, it will form a hydroxyl group with the bridging oxygen, making the aluminium a catalytically active Brønsted-site [15]. If however the charge is compensated by extraframework metal ions, such as extraframework alumina (EFAL), a lewis acid site is created [16]. A Lewis acid site is catalytically active in a different way, by polarizing the adsorbing reactant molecule and providing activation for the reaction to occur.


**Figure 2.2:** Brønsted and Lewis acid sites in zeolites. Adapted from Schulman et. Al. [2]

There are many different zeolite frameworks with different morphologies, porous structures and catalytic sites. Of all different zeolites, the two to be examined more closely in this thesis are Faujasite (FAU) and Mordenite (MOR). They are selected for catalysis based on their relatively large pores, faujasite with a catalytic pore size of 7.4 Å and mordenite with a pore size of 9-10 Å [17][18]. Both structures can have variation in aluminium content, and a full characterization of commercial zeolites includes stating the ratio of silicon to aluminium. For example, faujasite with a Si:Al-ratio of 6.05 silicon atoms per aluminium atom is specified as FAU 6.05.

The Si:Al-ratios in some commercial zeolites are given not as $Si/Al$ but as $SiO_2/Al_2O_3$, rather describing the silica-to-alumina ratio. It is important to keep this distinction in mind, since the silica-to-alumina ratio is twice that of the silicon to aluminium ratio, as it includes two aluminium atoms for every alumina in the ratio denominator. For consistency this thesis will depict all Si:Al ratios as $Silicon/Aluminium$.

### 2.2.1 Faujasite

Faujasite is one of the most common zeolites on the market due to its use in fluid catalytic cracking (FCC) and other hydrocarbon synthesis applications. Its importance has led to it being distinguished further in regard to its aluminium content, with faujasite of Si/Al ratios near 1 sometimes referred to as zeolite X while faujasites with a ratio higher than 2 are referred to as Zeolite Y. Faujasite finds such widespread use as a catalyst for fluid catalytic cracking due to its framework constituting strong Brønsted acid sites [16]. Faujasite pores are sinusoidally curved along the length of the pore.

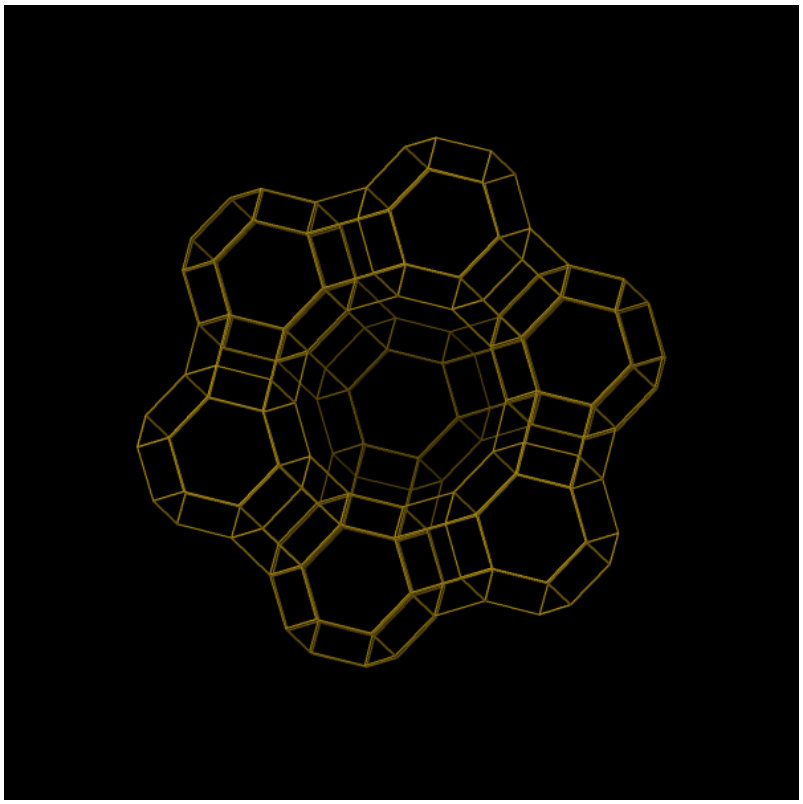

**Figure 2.3:** Faujasite crystal structure [3]

### 2.2.2 Mordenite

Mordenite is a useful zeolite for catalysis due to its large pores, its high surface area, its availability of both Brønsted- and Lewis acid sites, good thermal stability [19]. Mordenite contains two pore systems, one made up of 12-membered rings measuring 6.7 X 7 Å in an elliptical shape, as well as 8-membered rings measuring 3.4 X 4.8 Å. Since the 8-membered pores are relatively small, only the 12-membered pores are accessible for most organic molecules, and mordenite is therefore considered a 2-dimensional catalyst [20]. These pores are straight, as opposed to the sinusoidal pores of faujasite, which increases the degree of coking, deactivating mordenite faster during catalysis [17].

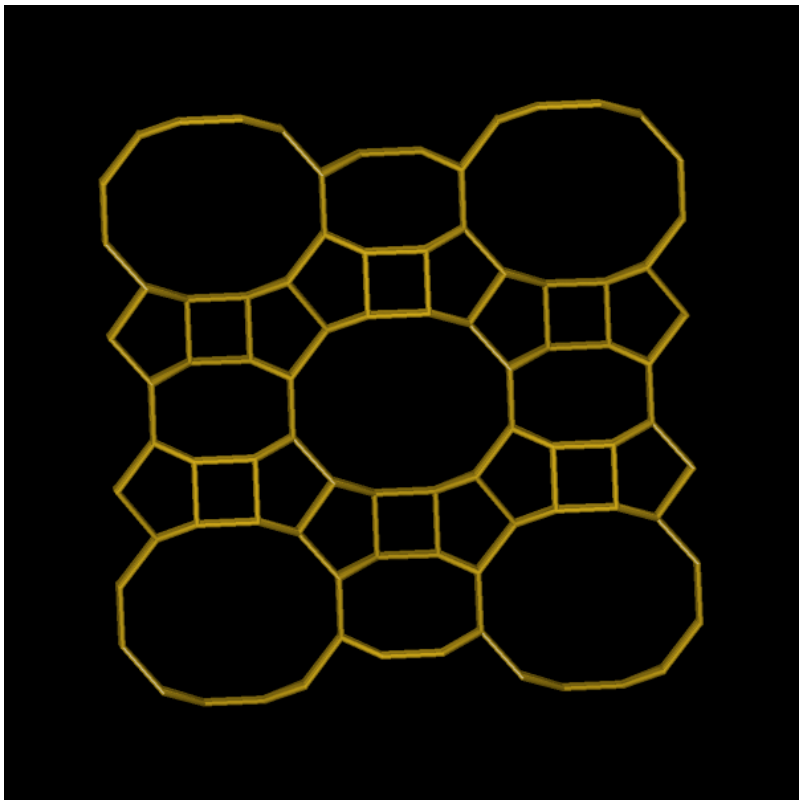

**Figure 2.4:** Mordenite crystal structure [4]

## 2.3 Zeolite post-synthesis modification

Some zeolites, such as zeolite Y cannot be directly synthesised with a high Si:Al ratio [21]. Therefore, post-synthesis modification is the only way to attain certain zeolites with a higher Si:Al ratio, such as ultrastable zeolite Y (USY). A widespread method of dealumination is high temperature steaming followed by mild acid leaching of extra-framework aluminium. An important aspect of dealumination is the structural stability of the framework. Removal of too much framework aluminium can lead to framework collapse and a reduction of catalytic activity.

The introduction of heteroatoms, such as gallium, in zeolites can be a useful tool in manipulating the catalytic properties to affect reactivity and catalyst lifetime [22]. The insertion of gallium in ZSM-5 frameworks increases the selectivity of hydrocarbon reaction towards aromatization [23], however, the mode of gallium insertion and the coordination of gallium in the framework entirely determines this effect[24]. After incipient wetness impregnation, most gallium species exists as aggregates of $Ga_xO_y$-particles on the surface of the zeolite, in aggregates the size of between 50-500 nm [25]. These aggregates are not very reactive in hydrocarbon aromatization and only a smaller amount of gallium will move into the structure to take a more active part in hydrocarbon conversion.

## 2.4 2,5-dimethylfuran

The model compound for a renewable BTX feedstock in this thesis will be 2,5-dimethylfuran (2,5-DMF). There are several factors for this choice of reagent. First, 2,5-dimethylfuran and many other furan compounds have been shown to be readily converted into BTX [26]. Second, 2,5-DMF can be readily produced from biomass, including cellulose rich waste products such as saw dust, agricultural byproducts, and sugar crops [12]. This could ensure a supply closer to the scale of global demand required for BTX production.

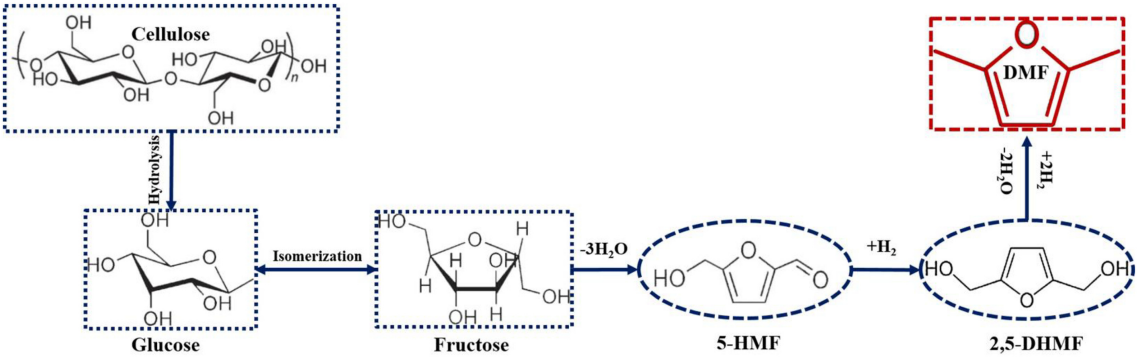


**Figure 2.5:** DMF synthesis from lignocellulosic biomass with HMF as an intermediate [5]

Thirdly, 2,5-DMF is relatively non-toxic compared to other furan compounds and thus preferrable to work with in a lab environment. While it may or may not be the most optimal furan for BTX aromatization, the use of a safe chemical as a model compound in a lab environment cannot be understated.

## 2.5 X-ray diffraction

X-ray diffraction is a powerful tool to examine the crystal structure of a compound by irradiating it with X-rays. X-rays are typically generated by shooting high energy electrons at a metal anode. The core shell electrons of the anode are ejected and outer electrons fill the vacancies, emitting high energy photons in the process. The photons' wavelengths are characteristic of the anode metal. The measurements in this thesis were done with a copper k-alpha anode, producing X-rays with a wavelength of 1.54Å.

The X-rays interact with the planes of the repeating unit cell, and are elastically scattered by the crystal lattice of the irradiated sample. Each repeating layer scatters more of the incident photons and soon all photons are reflected. The reflected light can then interact with itself and cause constructive interference at incident angles where the additional path travelled between layers equals a whole multiple of the photons wavelength, as depicted in figure 2.6. This causes certain angles, dependent on the photon wavelength, to register higher intensities at the detector. The angles are given by Bragg's law (equation 2.1) where $\theta$ is the incident angle, $\lambda$

the photon wavelength, $n$ is any positive integer and $d$ the distance between crystal planes.

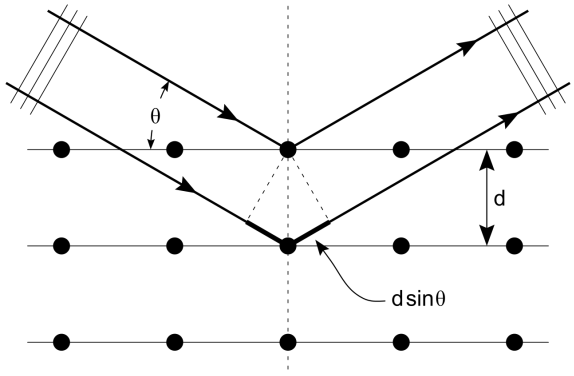


**Figure 2.6:** Bragg's law visualized [6]

$$n\lambda = 2dsin\theta \tag{2.1}$$

$$d = \frac{n\lambda}{2sin\theta} \tag{2.2}$$

Rearrangement of equation 2.1 gives 2.2 where $d$ is expressed as a function of $\theta$ and $\lambda$, both of which are known. Many different planes yield constructive interference over the varied incident angle and the resulting diffractogram is characteristic of the examined crystal unit cell, where different distances correspond to a set of crystallographic planes. X-ray diffraction is thus a useful way to determine that the zeolite produced is indeed crystalline. One can determine which zeolite structure is present and to some extent the degree of crystallinity.

## 2.6 Nitrogen physisorption

Nitrogen physisorption is used as a way of measuring surface area and pore volume of a solid substance. By step-wise introduction of a small amount of adsorbent gas, in this case nitrogen, one can measure the relative adsorbent gas pressure in the confined area surrounding the solid sample. The pressure difference can be used to determine the degree of adsorption, combined with a good model to correlate relative pressure and surface adsorption.

### 2.6.1 Langmuir theory

A useful but basic way to model the physisorption of a gas onto a surface is the Langmuir model, in which the relative coverage of a gaseous species onto a surface

can be described by

$$\Theta = \frac{\alpha * P}{1 + \alpha * P} \tag{2.3}$$

where $\Theta$ is the relative coverage of the surface, P the gas pressure and $\alpha$ is the Langmuir adsorption constant, dependant on the temperature and adsorption strength. Therefore, this equation is sometimes called the Langmuir Isotherm, as its behaviour depends on temperature.

The Langmuir equation makes a few assumptions, notably that all adsorption sites are thermodynamically equal, that each site can hold only one adsorbed molecule independent of its surroundings and, crucially, that adsorption occurs in a monolayer over the surface. Further refinement of the model can be done to account for multilayer adsorption which is an important component in the description of microporous adsorption.

### 2.6.2 BET model

The next step in the modelling of adsorption is the Brunauer-Emmett-Teller (BET) model. A new set of assumptions are used, namely that adsorption occurs in multilayers, one atop of another, infinitely. Next, the interaction between layers is negligible. Finally, Langmuir theory can be used to describe each independent layer. The result is the BET equation.

$$\Theta = \frac{c * P}{(1 - \frac{P}{P_0})(P_0 + P(c - 1))} \tag{2.4}$$

$\Theta$ is, similarly to the Langmuir equation, the degree of coverage, expressed still as a monolayer coverage. $P$ is the pressure, $P_0$ the saturation pressure and $c$ is a BET constant given by

$$c = \exp \frac{E_1 - E_L}{RT} \tag{2.5}$$

where $E_1$ is the heat of adsorption of the gas onto the solid and $E_L$ is the heat of adsorption of gas onto other gas molecules, i.e. multilayer adsorption.

Now, the BET equation can be rearranged into a more useful form, using the quantities $\phi = P/P_0$ as partial pressure, $v$ is the adsorbed gas volume and $v_m$ the volume of one adsorbed monolayer.

$$\frac{\phi}{v(1 - \phi)} = \frac{c - 1}{v_m c}\phi + \frac{1}{v_m c} \tag{2.6}$$

This equation can be plotted as a straight line, yielding the BET-plot used to calculate surface coverage. BET measurements usually exhibit a linear relation in the interval $0.05 < \phi < 0.35$. The straight line can be extrapolated to yield the line intercept and slope, providing a way to measure $v$ and $v_m$ respectively. Now $v_m$ can be used along with Avogadros number $N$, the cross section of one adsorbate molecule $s$, the molar volume of adsorbent gas $V$, and solid sample mass $m$ to finally get the specific surface area $S_{BET}$:

$$S_{BET} = \frac{v_m N s}{V} / m \tag{2.7}$$

This thesis will use specific surface area with the unit $m^2/g$.

### 2.6.3 The t-plot

To further qualify the determination of a samples surface area beyond the total surface area one can make use of the t-plot. It can be used to determine pore volume, pore area, and external surface area from the total surface area from the BET-plot. The t-plot method plots the adsorbed volume onto the surface against the adsorption layer thickness, using models of adsorbate thickness as a function of pressure. The results presented in this thesis have been determined using the de Boer model of adsorbate thickness. Linear regions in the t-plot behave as adsorption on a completely flat surface, and non-linear regions therefore indicate adsorption on non-flat surfaces, commonly pores. Y-axis intercept of the straight line gives the total volume of micropores. The rate at which adsorbent volume increases with adsorption layer thickness must then yield the adsorption area, and so the slope of the straight line indicates the area of non-porous adsorption. The difference between non-porous adsorption area and the total adsorption area from the BET calculation reveals the available microporous adsorption area.

## 2.7 Temperature programmed ammonia desorption

Potent acid sites are a necessary but not sufficient requirement for successful catalysis. Temperature programmed desorption of ammonia, or ammonia-TPD, can be used as a ways of measuring the number of acid sites in the examined zeolites. This is useful to determine the amount and strength of acid sites, giving an estimate of potential for successful catalysis.

Ammonia is an exceptionally "sticky" gas, and tends to chemisorb onto the available acid sites, forming -$NH_4^+$. After introducing ammonia to the sample and purging physisorbed ammonia, the amount of exiting ammonia as a function of temperature can then be measured in accurate ppm quantities, allowing for one to determine a precise amount of chemisorbed ammonia per milligram catalyst, and at what temperature the desorption occurs. Under the assumption that one ammonium molecule is bound per site one can calculate the acid site density of the catalyst.

Figure 2.7 shows a typical appearance of a ammonia TPD-plot, where concentration of ammonia and temperature are plotted as a function of time. As can be seen, several peaks can be fitted to approximate the shape of the desorption curve, making a reasonable assumption that the desorption profile can be said to consist of a number of discrete steps, representing a set of acid sites of different strength. The centre of the desorption peaks can be used to determine the temperature at which

the specific desorption steps occur. Three red peaks are fitted to the desorption ammonia concentration and their sum is shown as the blue line. The red ramping line indicates the temperature. The points where the grey vertical lines intersect the red temperature line gives the mean desorption temperature for each acid site.

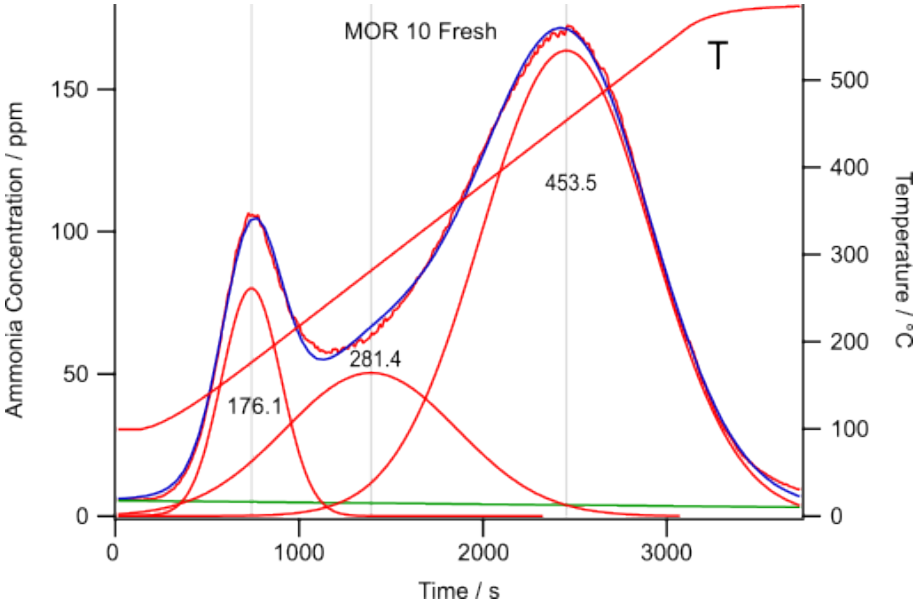


**Figure 2.7:** An example of a desorption profile.

Upon integration of these peaks one can determine the total amount of ammonia desorbed in ppm. By calculating the amount as a fraction of the total flow including both ammonia and argon carrier gas and using the ideal gas law, it is possible to calculate the number of ammonia molecules in mmol, and normalizing this number by the catalyst mass for each reaction experiment yields a final result of mmol acid sites / g catalyst.

# 3
# Methods

## 3.1 Catalysts

The zeolites were supplied by Alfa Aesar. They are presented in table 3.1.

| **Zeolite** | **FAU 2.55** | **FAU 6.05** | **FAU 15** | **FAU 30** | **MOR 10** |
|---|---|---|---|---|---|
| **Zeolite structure** | Faujasite | Faujasite | Faujasite | Faujasite | Mordenite |
| **Nominal cation form** | Ammonium | Ammonium | Hydrogen | Hydrogen | Ammonium |
| $SiO_2/Al_2O_3$ **mole ratio** | 5.1 | 12.1 | 30 | 60 | 20 |
| **Si:Al-ratio** | 2.55 | 6.05 | 15 | 30 | 10 |

**Table 3.1:** Zeolites used in reaction testing

These were used as catalysts for reaction tests. Dealumination and gallium insertion was performed with these zeolites as starting material.

## 3.2 Calcination

All catalysts were calcined before reaction testing. Some of the commercial zeolites used contain $NH_4^+$-counter ions. These must be exchanged with $H^+$-counter ions to make the zeolite acidic and catalytically active. $NH_4^+$ can be replaced with $H^+$ by heating the zeolite, calcining it, at 550°C under atmospheric conditions. The heat was ramped by 2°C per minute and held at 550°C for 5 hours.

## 3.3 Dealumination

Based on available equipment a method of dealumination was selected, involving only inorganic acid leaching, after a procedure of dealuminating zeolite Y proposed by Anggoro et. al. [27]. 1g of zeolite FAU6.05 was mixed in water along with 7M acid to a total volume of 10ml, and heated to 60°C for 2 hours in a sealed autoclave. The acids used where $H_2SO_4$ and $HNO_3$. The mixture was then rinsed over a filter with milliQ-water several times and freeze dried overnight.

Further attempts at dealumination by steaming in an autoclave proved unsuccessful.

## 3.4 Gallium insertion

Three different samples were selected for gallium ion exchange: FAU 2.55, FAU 6.05 and MOR 10. 1g of these samples was added to 12.5ml milliQ-water along with 0.1g Gallium nitrate ($Ga(NO_3)_3 \cdot H_2O$). The mixture was stirred continuously and heated to 60°C for 24 hours. The resultant mixture was vacuum filtered and rinsed repeatedly with milliQ-water. It was then freeze dried over night.

## 3.5 Mechanical catalyst preparation

Before reaction testing, the catalyst particles must be ensured to conform to a controlled size. Too large particles may influence the gas flow around and through the catalyst in the reactor, while too small particles might escape along with the carrier gas and contaminate the reactor. Therefore, catalyst samples were pressed in a hydraulic press under 10 MPa for 30 seconds and then ground in a mortar. The ground catalyst particles were then carefully sieved between two mesh sieves, the larger with a mesh size of 450 $\mu$m and the smaller with a mesh size of 355 $\mu$m.

## 3.6 X-ray diffraction

The instrument used for the results in this thesis was of model Bruker D8 Discover. It used a Cu K$\alpha$ radiation source with a non-rotating sample, a fixed illumination area of 5mm, a 1mm distance from sample to a shielding anti-scatter knife and a scan time of 1 s per step, scanning in increments of $0.02^o$ $2\theta$. The detector used was an Eiger2R 500K. The data was treated by removal of the background baseline.

## 3.7 Nitrogen physisorption

The instrument used for nitrogen physisorption was of model TriStar II Plus. Before measurement, the samples were pretreated by degasing under argon flow at 500 °C. The points for the resultant BET plot were selected to satisfy the Roquerol criteria. The thickness range for the t-plot was between 4 and 12 Å for all samples.

## 3.8 Reaction testing and flow reactor setup

The flow reactor for catalyst performance testing (see figure 3.1) consists of three main parts: One bank of mass flow controllers, MFCs, for accurate flow regulation of three different gasses. Argon is used as a carrier gas, ammonia for temperature programmed desorption, and oxygen for catalyst regeneration/oxidation of coke species in the reactor. The total gas flow under operation of the reactor is 300ml/min. A fourth MFC directs argon through a glass bubbler, wherein the reactant liquid resides. As argon flows through the bubbler it will disperse a small amount of reactant into a fine mist which can be carried into the reactor.

The second main part of the reactor setup is the reactor itself. It consists of the reactor tube in which the catalyst resides, and a heating coil that can accurately determine the temperature of the catalyst bed. The glass reactor tube contains 50-100 mg of catalyst particles contained between two sections of approximately 40 mg glass wool, to ensure that the catalyst particles stay in the tube. Within the reactor tube there are two thermocouples to determine the temperature, one within the catalyst mass and one slightly above, which makes it possible to regulate the temperature based both on temperature data from the heating coils and from exothermic or endothermic reactions over the catalyst. The reaction temperature was set to 500 ℃and the reaction went on for 8 hours. Afterwards, the catalyst was regenerated at 625 ℃in 3% oxygen for 30 minutes, burning away the soft coke, followed by 45 minutes in 20% oxygen to remove remaining hard coke.

The last main part of the flow reactor is situated just after the reactor tube. The gas flow can be directed either to the exhaust or to an on-line IR instrument for determining the composition of the gas exiting the reactor. This is where all reaction measurements and ammonia TPD measurements are made. The reactor was also equipped with an on-line mass spectrometer, which could be used to confirm products in low quantities. However, due to the complex fragmentation pattern of the gas mixture, and the fact that interest was focused on products of high enough quantity to be within the range of IR detection, the mass spectrometer measurements have been omitted from this thesis.

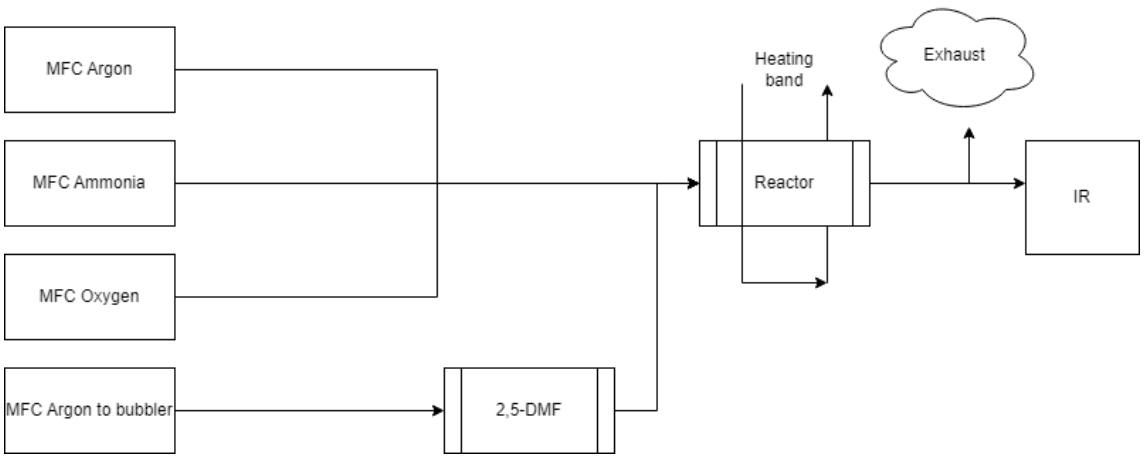


**Figure 3.1:** Schematic of flow reactor

To determine conversion of 2,5-DMF and selectivity toward BTX from the gas composition data, the following calculations were made: First, the concentration of all reactants was calculated as a fraction of 2,5-DMF carbon content. $C_{prod}$ is the concentration of all products normalized after 2,5-DMF carbon content, $n_i$ is the carbon atom count of each product, and $n_{DMF}$ the carbon count of 2,5-DMF = 6

$$C_{prod} = \sum \frac{n_i}{n_{DMF}} \tag{3.1}$$

Now, as $C_{prod}$ is expressed in equivalents of converted 2,5-DMF one can write

$$Conversion = \frac{C_{prod}}{C_{prod} + DMF} \tag{3.2}$$

To get a measure of how much 2,5-DMF has been converted at any given concentration of products and reactants.

Selectivity is calculated by equation 3.3:

$$S_{BTX} = \frac{C_{BTX}}{C_{prod}} \tag{3.3}$$

where $C_{BTX}$ is the concentration of a specified BTX-species (or the total BTX concentration) at any given time.

When conversion gets too low the formula for selectivity will give unreliable results, as its denominator, conversion, approaches 0. This will occasionally cause the selectivity to spike at low conversion, as can be seen for example in figure 4.6a. The results have been included for the whole first hour to be visible for each reaction, but it is advised to be critical when examining selectivities at low conversion.

## 3.9 Temperature programmed ammonia desorption

The catalyst bed was dried and purged of any atmospheric gasses, whereupon ammonia in a small quantity mixed with argon as a carrier gas was flowed through the catalyst bed. Down the stream the gas was continuously monitored via on-line FTIR. After 1h the gas stream was then switched to pure argon and was allowed to purge for a while, to make sure that only chemisorbed ammonia was left in the reactor. Then the temperature was raised, with a ramping temperature increase of 10 °C per minute. The temperature was raised to 600 ℃, and the emerging gas mixture was measured in the FTIR.

# 4

# Results and discussion

## 4.1 Catalyst characterization

### 4.1.1 X-ray diffraction

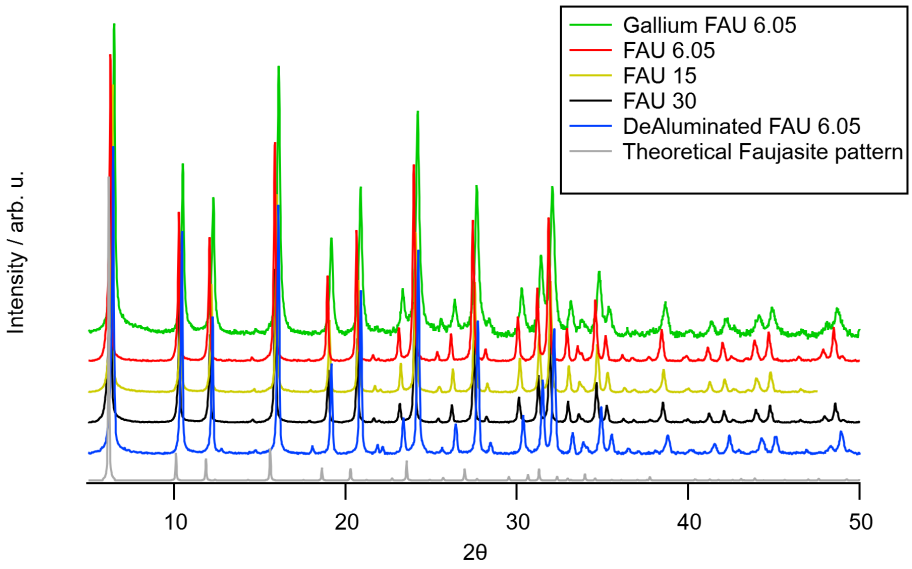


**Figure 4.1:** X-ray diffraction pattern of FAU 6.05, 15, 30, Dealuminated FAU 6.05 and Gallinated FAU 6.05, along with a calculated faujasite pattern

The diffraction patterns in figure 4.1 show similar appearance for most faujasites. The sharp peaks indicate a regular lattice for all faujasites, including the dealuminated sample which has been subjected to the harshest conditions. Some peak broadening can be observed for the gallinated FAU 6.05. The diffractogram for FAU 2.55 has been included in its own figure due to its unique appearance.
In figure 4.2 can be seen the diffraction patterns for the two FAU 2.55-samples. The peaks intensities are lower as compared to faujasite in figure 4.1 which can be seen by the higher noise in the baseline. In fact, it appears that some baseline drift might have remained after background elimination, as it cannot be completely separated from the noise.
All gallium treated samples show a systematic peak shift slightly toward higher angles. This is due to a different sample holder being used for these samples. Gallium mordenite shows a relative intensity shift toward lower angles, which could indicate a pore widening.

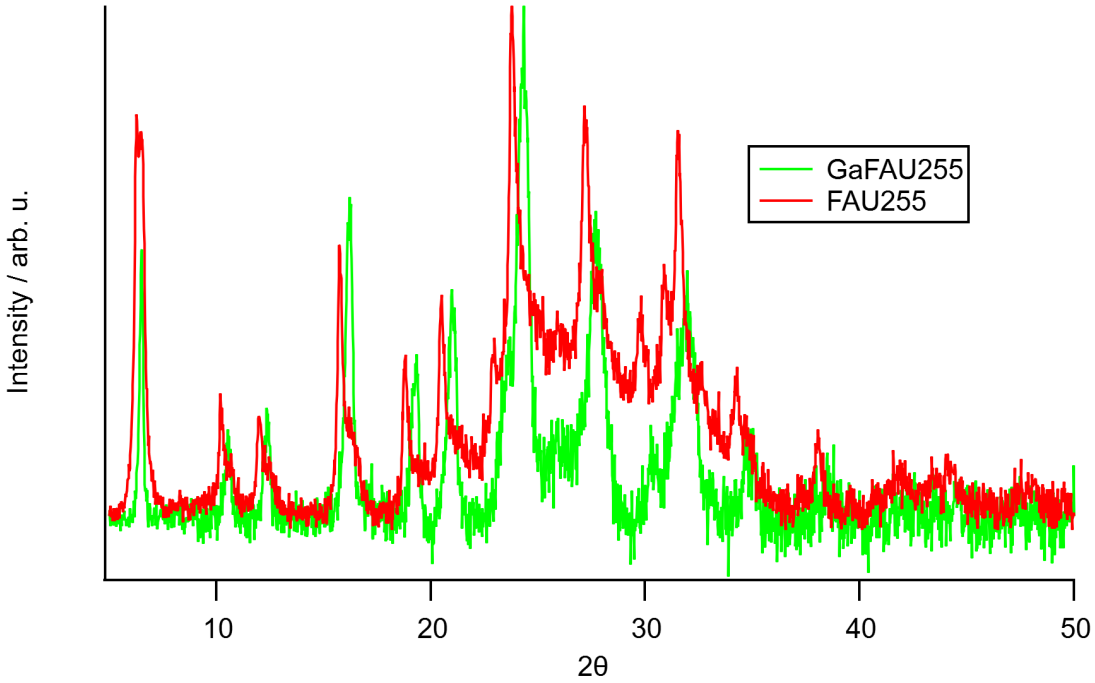


**Figure 4.2:** X-ray diffraction pattern of FAU 2.55 and gallinated FAU 2.55

The diffractogram of mordenite samples in figure 4.3 shows sharp and well distinguished peaks. There might be some degree of peak broadening in the gallinated mordenite sample, but it is to a lower extent than that observed in figure 4.1.

### 4.1.2 Nitrogen physisorption

The results of catalyst surface area and porosity measurements are presented in table 4.1.

| Sample | Micropore volume $cm^3/g$ | Micropore area $m^2/g$ | External surface area $m^2/g$ | Total surface area $m^2/g$ |
|---|---|---|---|---|
| **FAU 2.55** | 0.113 | 295.82 | 9.92 | 305.74 |
| **GaFAU 2.55** | 0.081 | 209.30 | 10.70 | 220.00 |
| **FAU 6.05** | 0.251 | 637.91 | 64.77 | 702.68 |
| **GaFAU 6.05** | 0.193 | 485.22 | 61.94 | 547.17 |
| **MOR 10** | 0.213 | 553.29 | 22.98 | 576.27 |
| **GaMOR 10** | 0.181 | 471.39 | 28.02 | 499.42 |
| **FAU 15** | 0.330 | 815.13 | 79.52 | 894.65 |
| **FAU 30** | 0.306 | 740.68 | 74.92 | 815.60 |
| **Dealuminated FAU6.05** | 0.325 | 796.90 | 86.57 | 883.47 |

**Table 4.1:** Physisorption data for all samples

There are a few trends to be noted in table 4.1: Firstly, gallinated samples show a decrease in micropore volume and area compared to their non-gallinated counterparts. Gallinated FAU 2.55 and Gallinated MOR 10 also show an increase in external surface area, while gallinated FAU 6.05 shows a decrease. Furthermore, with an increasing Si:Al-ratio one can see an increase in micropore volume, micropore area, external surface area, and total surface area for faujasite, until it decreases at Si:Al ratios higher than 15. Lastly, the dealuminated FAU 6.05-sample shows a

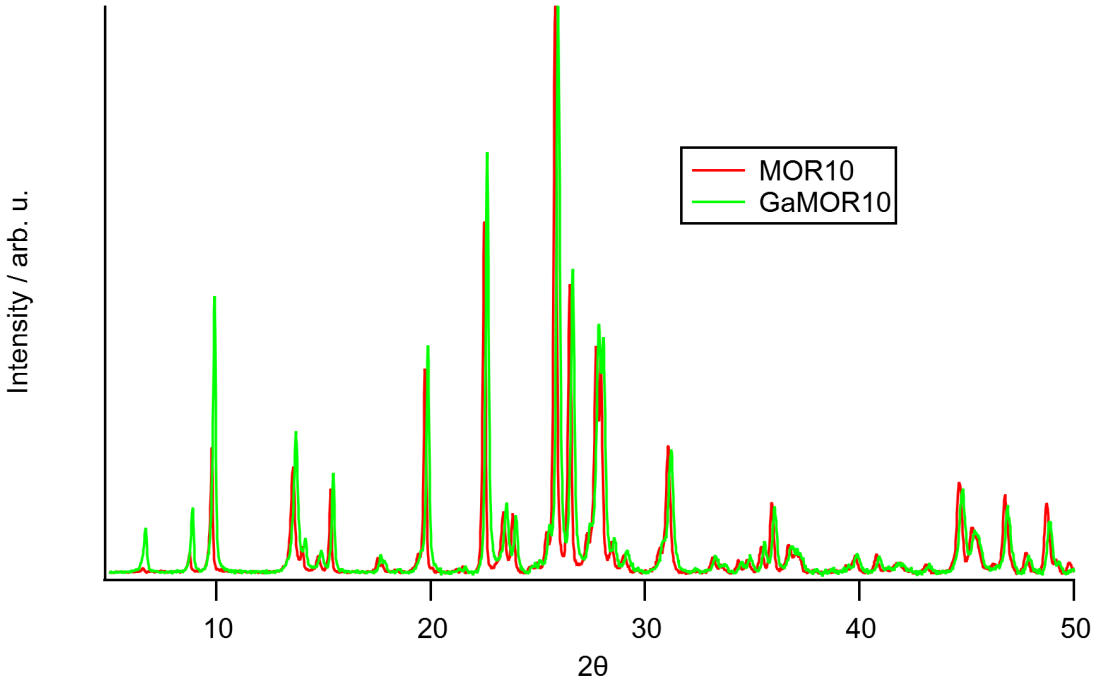


**Figure 4.3:** X-ray diffraction pattern of MOR 10 and gallinated MOR 10

porosity and surface area profile highly similar to that of FAU 15.

### 4.1.3 X-ray fluorescence

The Aluminium and gallium contents were confirmed with x-ray fluorescence after treatment. The results are presented in table 4.2

| Catalyst | FAU 2.55 | GaFAU 2.55 | FAU 6.05 | GaFAU 6.05 | MOR 10 | GaMOR 10 | DeAl FAU 6.05 |
|---|---|---|---|---|---|---|---|
| **Silicon wt%** | 31.64 | 32.09 | 39.10 | 39.70 | 41.64 | 41.65 | 44.02 |
| **Aluminium wt%** | 11.38 | 12.06 | 6.06 | 5.35 | 3.84 | 3.66 | 1.09 |
| **Gallium wt%** | n/a | 3.43 | n/a | 3.53 | n/a | 2.26 | n/a |
| **Si:Al-ratio** | 2.67 | 2.62 | 6.20 | 7.13 | 10.42 | 10.94 | 38.74 |
| **Si:Ga-ratio** | n/a | 23.83 | n/a | 27.90 | n/a | 45.79 | n/a |

**Table 4.2:** Silicon, aluminium, and gallium content of treated zeolites and their untreated counterparts

The Si:Al-ratio of the dealuminated sample is determined to be 40. The zeolite has been extensively dealuminated, and is the most siliceous out of all examined catalysts. All purchased zeolites are confirmed to have an aluminium content close to what is specified by the supplier within a small margin of error.

Gallium insertion is confirmed to have had the desired effect of depositing gallium within the treated zeolites. Mordenite has had the least retained gallium, which can be attributed to it having smaller pores.

## 4.2 Temperature programmed ammonia desorption

The amount of acid sites is overall consistent with the degree of conversion of 2,5-DMF.

| Catalyst | Acid sites before reaction $mmol/g$ | Acid sites after reaction $mmol/g$ | Loss $mmol/g$ |
|---|---|---|---|
| **FAU 2.55** | 0.292 | 0.221 | 0.071 |
| **GaFAU 2.55** | 0.362 | 0.261 | 0.101 |
| **FAU 6.05** | 0.479 | 0.412 | 0.067 |
| **GaFAU 6.05** | 0.468 | 0.384 | 0.084 |
| **MOR 10** | 0.863 | 0.803 | 0.060 |
| **GaMOR 10** | 0.921 | 0.816 | 0.105 |
| **FAU 15** | 0.379 | 0.322 | 0.057 |
| **FAU 30** | 0.198 | 0.189 | 0.009 |
| **DeAl FAU 6.05** | 0.039 | 0.058 | -0.019 |

**Table 4.3:** Acid sites before and after reaction testing

In figure 4.4 is displayed the plots of multi-peak fitting for ammonia TPD. The first set of six graphs depict the desorption profiles for the first three catalysts before and after reaction testing. The second set depicts the desportion profiles for FAU 15, FAU 30 and dealuminated FAU 6.05. The last set of graphs depict desorption profiles for the gallium treated samples. For faujasites, a reduction in aluminium reduces the abundance of all acid sites, but it seems to affect weak acid sites especially. Less aluminium consistently increases desorption temperature for all peaks, and increases the relative abundance of especially the middle strength acid sites. Gallium reduces the overall acidity of FAU 6.05 but increases acidity of FAU 2.55 and MOR 10. Interestingly enough, the weak acid sites seem to be particularly increased by gallium. The desorption of FAU 6.05 is not easily approximated by only three peaks, but this was done for sake of comparison between samples.

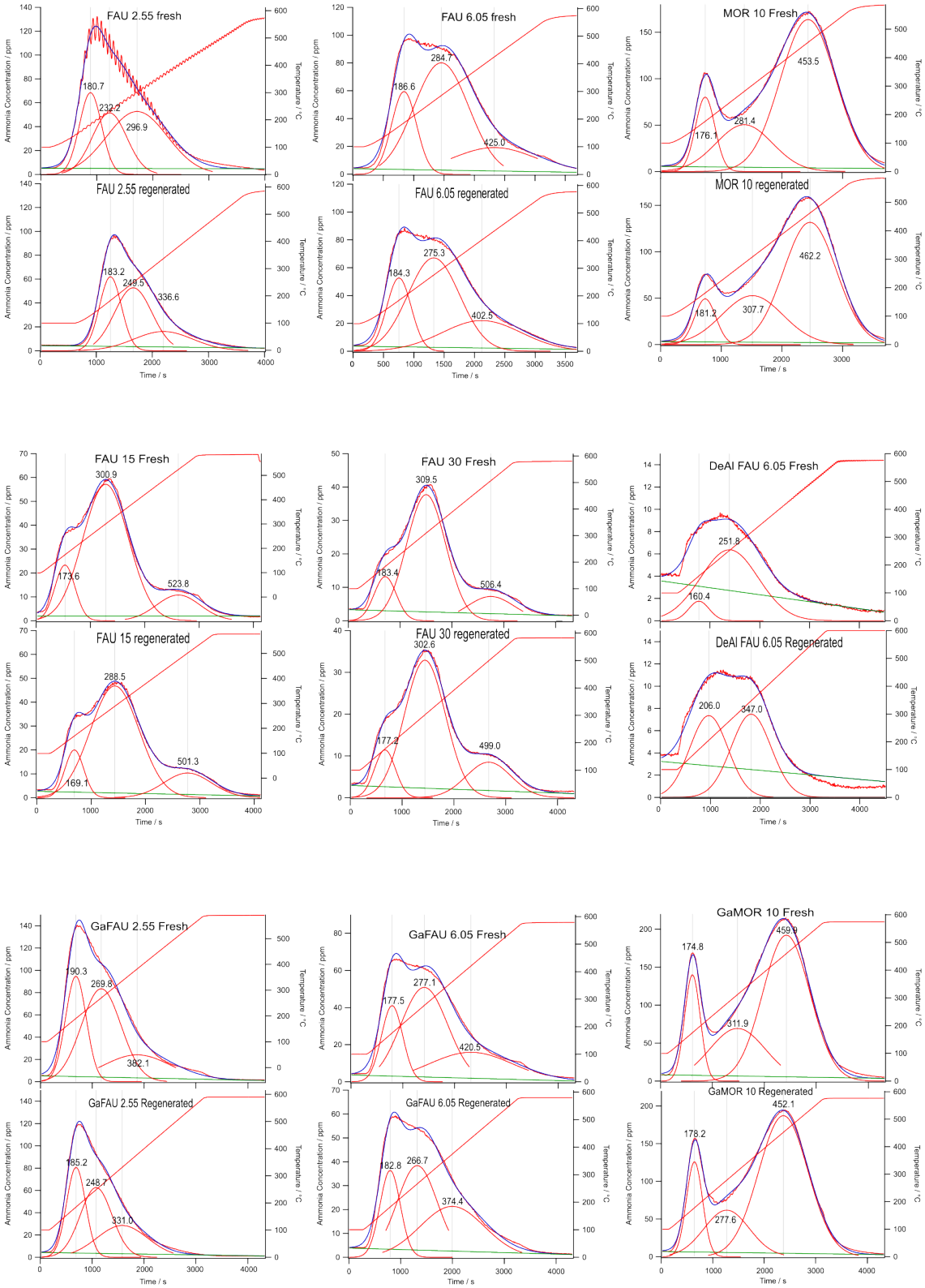


**Figure 4.4:** Acid site profiles before and after reaction testing

## 4.3 Reaction testing

The reaction tests are presented in three sections. First, the results of the initial testing of the untreated FAU 2.55, FAU 6.05 and MOR 10 are shown in comparison. Next, the reaction testing results are shown for all faujasites of varying aluminium content. Last, the reaction testing results of gallium treated samples are displayed.

### 4.3.1 Initial reaction testing

The concentration of all products is presented in figure 4.5 for the first hour after introduction of 2,5-DMF over the catalyst. The catalyst is rapidly deactivated and reaches a steady state for most products within an hour. This method of data presentation is messy, and alterations were made for presentational clarity. The conversion of 2,5-DMF and its selectivity towards benzene and toluene will be used as a measure of performance for each catalyst. The selectivity toward xylenes is near zero for all catalysts and has been omitted from total BTX as it would add mostly noise to the signal.

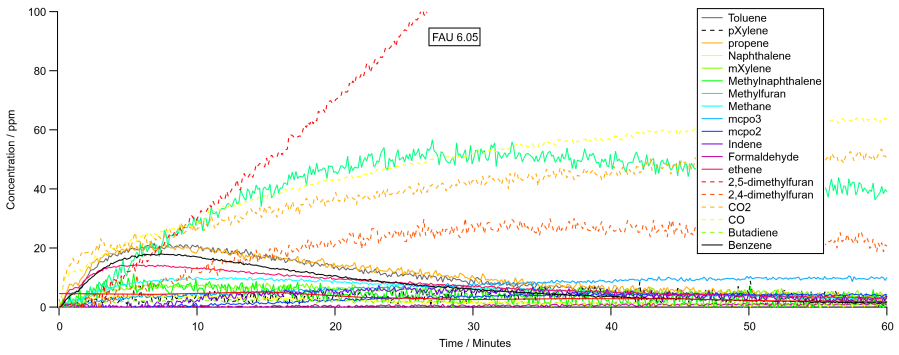


**Figure 4.5:** All detected products for one hour after reaction

In figure 4.6 can be seen the reaction testing results of initial catalysts.

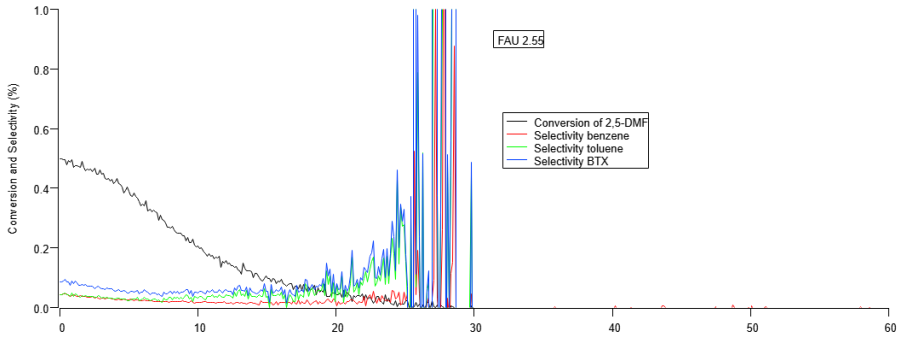


**(a)** FAU 2.55

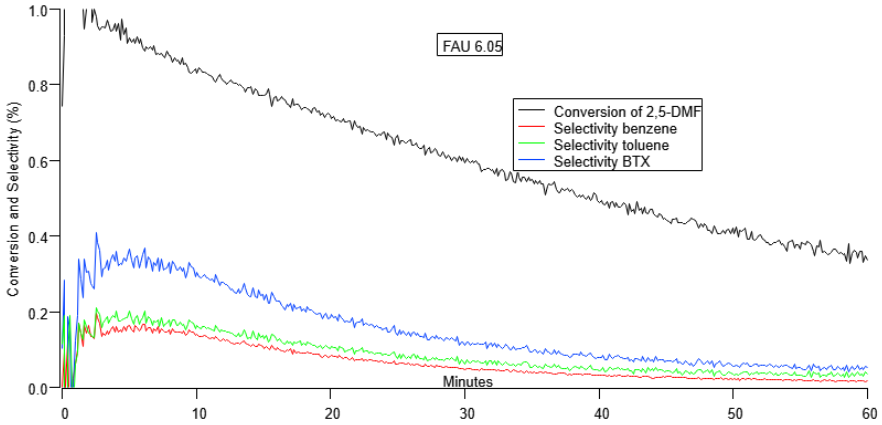


**(b)** FAU 6.05

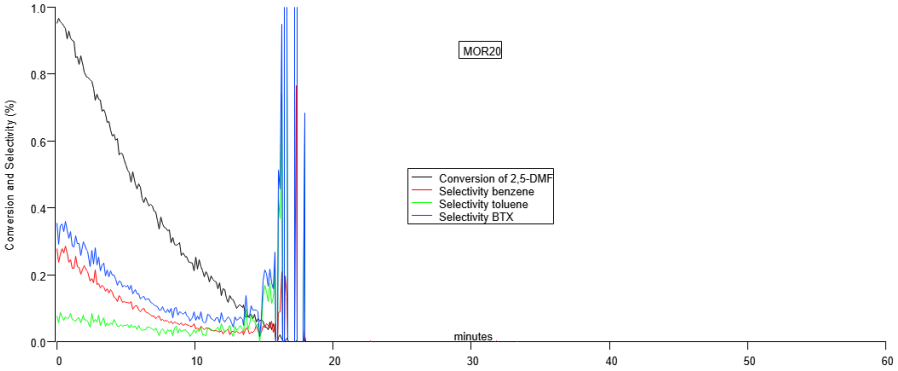


**(c)** MOR 10

**Figure 4.6:** Conversion of dimethylfuran and reaction selectivity towards benzene, toluene and BTX during the first hour of reaction after introduction of dimethylfuran over the catalyst.

### 4.3.2 Reaction as a function of aluminium content in faujasite

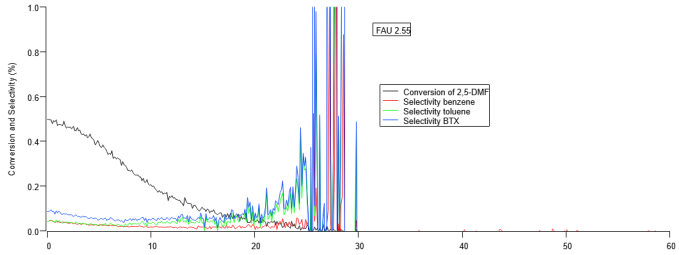


**(a)** FAU 2.55

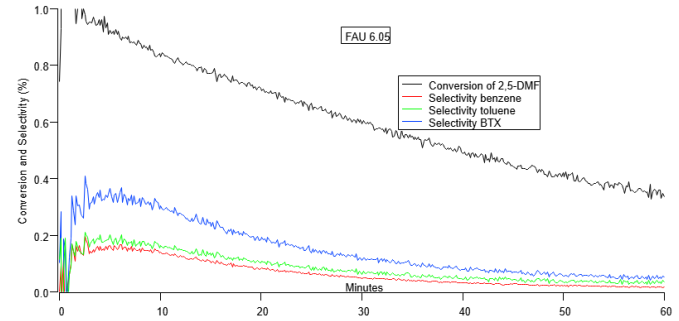


**(b)** FAU 6.05

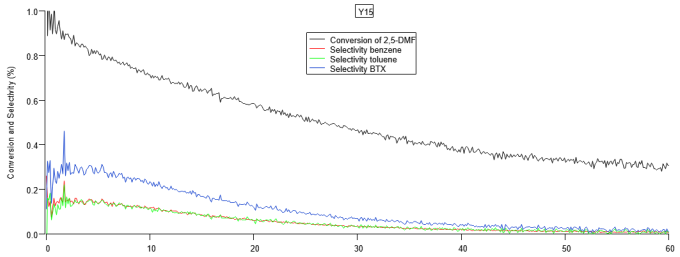


**(c)** FAU 15

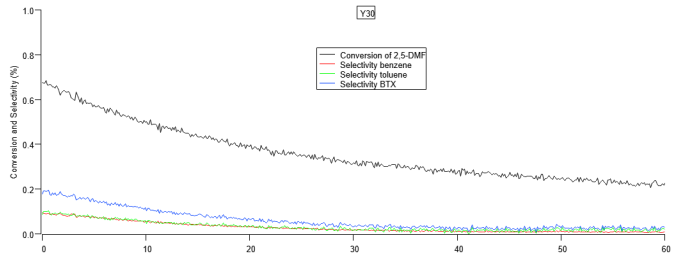


**(d)** FAU 30

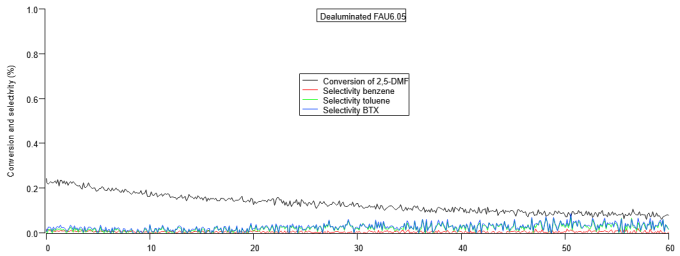


**(e)** Dealuminated FAU 6.05

**Figure 4.7:** Conversion of dimethylfuran and reaction selectivity of BTX for different aluminium content in faujasite

Reaction testing was performed over faujasites with Si:Al ratios of 2.55, 6.05, 15, 30 and the dealuminated 6.05 with a ratio of 38.74.

In figure 4.7a FAU 2.55 shows comparatively low initial conversion and and selectivity, and a realtively swift deactivation of catalyst, having reached 0 conversion before 30 minutes. FAU 6.05 and 15 in figures 4.7b and 4.7c show a similar behaviour to one another, with a high initial conversion, a high selectivity and a reasonably slow decline of conversion. Both FAU 6.05 and FAU 15 seem to reach a conversion of 40% after 60 minutes of reaction, however FAU 6.05 is somewhat distinguished by a slightly higher initial selectivity, favouring toluene. In figure 4.7d FAU 30 shows a somewhat low initial conversion and selectivity, with a slower decline in both, as compared to FAU 2.55, and with a conversion reaching around 30% after 60 minutes. Finally, the dealuminated FAU6.05 sample in figure 4.7e shows the lowest initial conversion, and no selectivity toward BTX to speak of. Its final conversion is close to its initial conversion.

Out of all the faujasites, FAU 6.05 seems to be the best performing catalyst. It is however interesting to note how a reduction in aluminium content to about half of that of FAU 6.05 still performs in a similar way. The drop in conversion and selectivity is much more dramatic upon halving the aluminium content again, from FAU 15 to FAU 30, and near total in reducing the aluminium content from a ratio of 30 to a ratio of 38.74.

The performance of FAU 2.55 is difficult to gauge, as it seems to perform worse due to several different reasons. First, a higher aluminium content influences the balance of Brønsted and Lewis acid sites, as more aluminium is present as EFAl. The low conversion could also be attributed to it being more amorphous, as indicated by the low relative intensities in XRD and the low measured micropore area and volume. Thus, determining its reactivity as a function of aluminium content becomes difficult. Aluminium at this low Si:Al-ratio influences reactivity in more ways than just the number of sites.

### 4.3.3 Reaction testing for gallinated samples

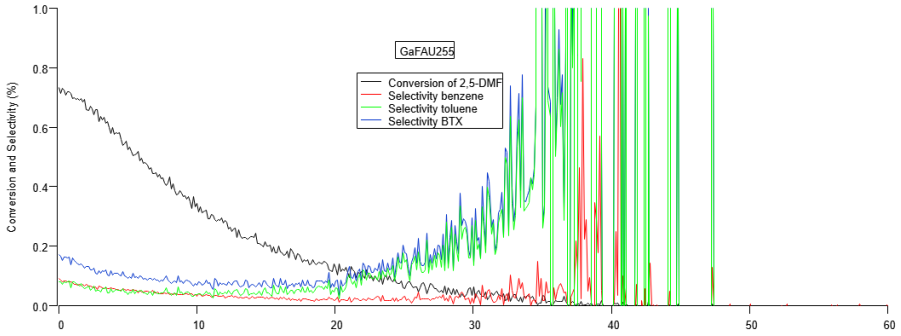


**(a)** Gallium FAU 2.55

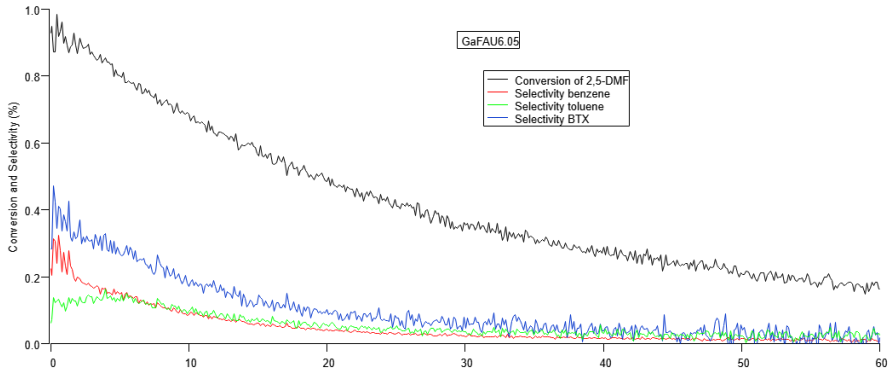


**(b)** Gallium FAU 6.05

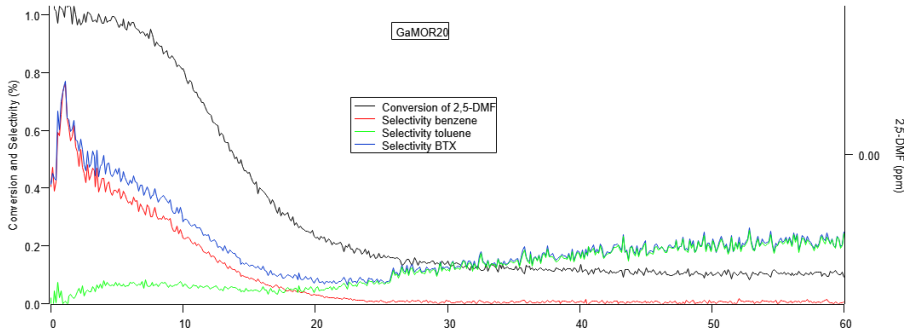


**(c)** Gallium MOR 10

**Figure 4.8:** Conversion of dimethylfuran and reaction selectivity towards benzene during the first hour of reaction for gallium exchanged samples

The reaction testing after gallination of FAU 2.55, depicted in figure 4.8a shows most notably that the initial conversion is greater than that found in figure 4.6a. Initial selectivity toward BTX is also higher, though relatively low overall. Gallium FAU 6.05 in figure 4.8b shows a similar result as its ungallinated counterpart. The selectivity of Gallium FAU 6.05 seems to be initially slightly more favoured toward benzene, while toluene selectivity is proportionally unfavoured. Gallium MOR 10 in figure 4.8c displays notable differences compared to its ungallinated counterpart

in figure 4.6c. Its initial conversion of 100% is sustained for longer, until it falls rapidly. It does not fall to 0, but stays at above 15%. The initial conversion lies briefly above 60% and is entirely favoured toward benzene. As conversion drops its selectivity becomes favoured entirely toward toluene, and the gallinated MOR 10 shows the unique property of having a BTX selectivity that approaches a non-zero value as 60 minutes have passed. A low but non-zero conversion can also be seen after 60 minutes. This conversion and selectivity is even maintained for the full 8 hours of reaction, shown in figure 4.9.

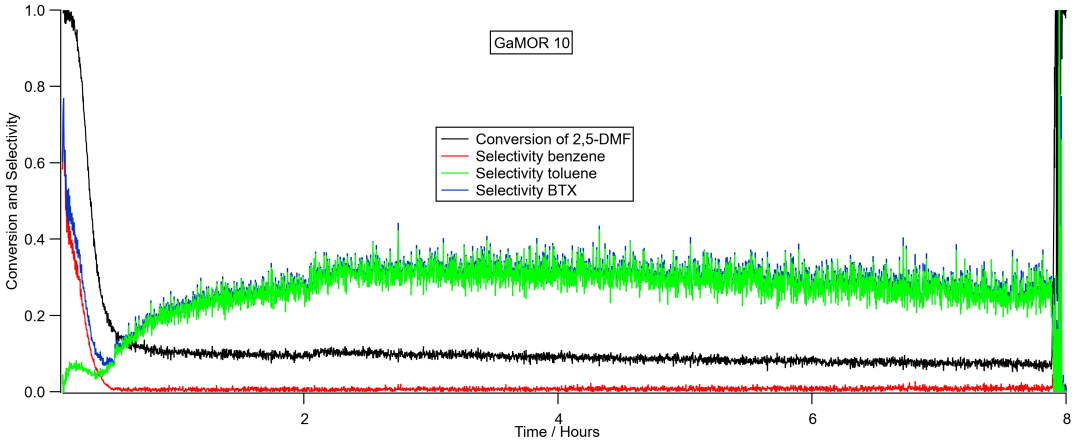


**Figure 4.9:** Gallium Mordenite selectivity and conversion for 8 hours of reaction

Gallination of the three examined catalysts resulted in a lower micropore area and volume. This is to be expected, as gallium species could end up within the pores and block available space for reaction species. However, the amount of acid sites are increased for FAU 2.55 and MOR 10 but not for FAU 6.05. An increase in reaction conversion and selectivity is noted in those catalysts where acid sites are increased. This leads to one possible conclusion that gallium can increase acidity, and thus performance, of zeolites. An important question arises from this: why does this not happen for FAU 6.05? GaFAU 6.05 does after all have a higher Si:Ga-ratio than the clearly affected GaMOR. Gallium treatment does have one visible effect on FAU 6.05, namely that the initial selectivity is more favoured toward benzene at the expense of toluene selectivity. The effects of gallium extend further than simply increasing acidity of the zeolite.

Gallium ion exchange generally does not create catalytically active sites where there is only silica. It must either take the place of framework aluminium or reside in an extra-framework position. The gallination was attempted to exchange framework aluminium with gallium but the decrease in porosity tells that some, if not most of the gallium is present outside the framework.

Determining exactly the coordination and character of gallium or aluminium in the zeolite structure is beyond the scope of this thesis as it cannot be determined without NMR spectroscopy or similar methods. In improving upon these results, one could strive to categorize the full character of aluminium and gallium in sam-

ples like these in order to determine what role EFAl and EFGa play in reactivity, compared to their framework counterparts.

Another interesting result from gallium treatment is the extension of catalyst lifetime of mordenite. Gallium could prevent the formation of some coke species, even to such an extent as to make mordenite retain some activity for several hours. The selectivity being relatively high towards toluene, but non-existent towards benzene is also noteworthy for future studies.

One way of improving the effect of gallium insertion is to have the gallium-exchanged sample undergo reduction/oxidation cycles [28]. Since surface gallium aggregates are a problem with gallium insertion, one way of allowing gallium to migrate deeper into the framework is to reduce it in a hydrogen atmosphere at temperatures above 500 °C. The $GaH_2$ species is less bulky and can traverse through the network easier. Once inside, they can again be oxidized to form the catalytically active $Ga_xO_y$ species. Studying the effect of more thorough gallium insertion would be interesting moving forward. Similarly, the gallium retention of dealuminated faujasite would be of interest to study. It is possible that thorough dealumination can create vacancies in the framework, which can be stabilized by gallium, ensuring that more gallium is retained and to a higher degree in framework positions. An attempt was made for this thesis to insert gallium into the dealuminated FAU 6.05, but too little sample remained for there to be enough for reaction testing.

# 5
# Conclusion

In this thesis I have studied the impact of aluminium and gallium content on the performance of catalysts in converting 2,5-dimethylfuran into benzene, toluene and xylene. Crystal structure was studied with x-ray diffraction, porosity was studied with nitrogen physisorption, aluminium and gallium content was studied with x-ray fluorescence spectroscopy and acidity was studied via temperature-programmed ammonia desorption. Catalyst performance was evaluated in a flow reactor setup, determining products with on-line infrared spectroscopy.

The findings of this thesis imply that there is an optimum aluminium content of faujasite for BTX production from 2,5-DMF. A balance of amount and strength of acid sites must be found for optimal catalysis. A Si:Al-ratio of 6.05 was the best performing of the ones examined in this thesis, but it is possible that even greater conversion and selectivity can be found somewhere between the ratios 2.55 and 15.

Gallium added to the zeolites can improve the performance of BTX production and influence the favour of selectivity toward different BTX compounds.

Moving forward, it is of interest to determine how the framework integration of aluminium and gallium influences the selectivity and conversion. Methods to measure and influence this is of interest for further studies.

All in all, the most interesting catalyst for production of BTX is gallium mordenite. The short lifetime can be counteracted by continuous catalyst regeneration, making the high conversion and selectivity most significant. A conversion of 100% and a selectivity of 40% could be sustained for far longer, giving a promising catalyst for BTX production.

# Bibliography


[1] S. Top and H. Vapur, "Türk termik santrallerinden iki farkli uçucu kül kullanarak alkali yakma metoduyla zeolit sentezi," *Bilimsel Madencilik Dergisi*, vol. 59, pp. 7–14, 03 2020.

[2] E. Schulman, W. Wu, and D. Liu, "Two-dimensional zeolite materials: Structural and acidity properties," *Materials*, vol. 13, no. 8, 2020. [Online]. Available: https://www.mdpi.com/1996-1944/13/8/1822

[3] I. Z. Association, "Framework type fau," 2023. [Online]. Available: https://europe.iza-structure.org/IZA-SC/framework_3d.php?STC=FAU

[4] ——, "Framework type mor," 2023. [Online]. Available: https://europe.iza-structure.org/IZA-SC/framework.php?STC=MOR

[5] X. P. Nguyen, A. T. Hoang, A. I. Ölçer, D. Engel, V. V. Pham, and S. K. Nayak, "Biomass-derived 2,5-dimethylfuran as a promising alternative fuel: An application review on the compression and spark ignition engine," *Fuel Processing Technology*, vol. 214, p. 106687, 2021. [Online]. Available: https://www.sciencedirect.com/science/article/pii/S0378382020309784

[6] user Hydrargyrum, "X-ray crystallography," 2023. [Online]. Available: https://en.wikipedia.org/wiki/X-ray_crystallography#/media/File:Bragg_diffraction_2.svg

[7] I. Markit, "Distribution of primary petrochemical consumption worldwide in 2021," 2021. [Online]. Available: https://www.statista.com/statistics/1319374/petrochemical-consumption-share-by-type-globally/

[8] SA, "Aromatics btx production cost 2023-2028: Price trends analysis, profit margins, plant cost, industry trends," 2023. [Online]. Available: https://www.marketwatch.com/press-release/aromatics-btx-production-cost-2023-2028-price-trends-analysis-profit-margins-plant-cost-indus

[9] OEERE, "Energy and environmental profile of the u.s. chemical industry," 2000. [Online]. Available: https://web.archive.org/web/20120904145814/http://www1.eere.energy.gov/manufacturing/industries_technologies/chemicals/pdfs/profile_full.pdf

[10] S. Matar and L. F. Hatch, "Chapter ten - chemicals based on benzene, toluene, and xylenes," in *Chemistry of Petrochemical Processes (Second Edition)*, second edition ed., S. Matar and L. F. Hatch, Eds. Woburn: Gulf Professional Publishing, 2001, pp. 262–300. [Online]. Available: https://www.sciencedirect.com/science/article/pii/B9780884153153500110

[11] C. Sauer, A. Lorén, A. Schaefer, and P.-A. Carlsson, "Valorisation of 2,5-dimethylfuran over zeolite catalysts studied by on-line ftir-ms gas phase

analysis," *Catal. Sci. Technol.*, vol. 12, pp. 750–761, 2022. [Online]. Available: http://dx.doi.org/10.1039/D1CY01312B

[12] Y. Román-Leshkov, C. J. Barrett, Z. Y. Liu, and J. A. Dumesic, "Production of dimethylfuran for liquid fuels from biomass-derived carbohydrates," *Nature*, vol. 447, no. 7147, pp. 982–985, Jun 2007. [Online]. Available: https://doi.org/10.1038/nature05923

[13] R. E. Fletcher, S. Ling, and B. Slater, "Violations of löwenstein's rule in zeolites," *Chem. Sci.*, vol. 8, pp. 7483–7491, 2017. [Online]. Available: http://dx.doi.org/10.1039/C7SC02531A

[14] J. Antúnez-García, D. Galván, V. Petranovskii, F. N. Murrieta-Rico, R. I. Yocupicio-Gaxiola, M. G. Shelyapina, and S. Fuentes-Moyado, "Aluminum distribution in mordenite-zeolite framework: A new outlook based on density functional theory calculations," *Journal of Solid State Chemistry*, vol. 306, p. 122725, 2022. [Online]. Available: https://www.sciencedirect.com/science/article/pii/S0022459621007702

[15] M. Ravi, V. L. Sushkevich, and J. A. van Bokhoven, "Towards a better understanding of lewis acidic aluminium in zeolites," *Nature Materials*, vol. 19, no. 10, pp. 1047–1056, Oct 2020. [Online]. Available: https://doi.org/10.1038/s41563-020-0751-3

[16] S. Almutairi, "The role of lewis and brønsted acidity for alkane activation over zeolites," Ph.D. dissertation, Technische Universiteit Eindhoven, type = PhD thesis, 2013, https://doi.org/10.6100/IR755379.

[17] S. Prodinger and M. A. Derewinski, "3 - synthetic zeolites and their characterization," in *Nanoporous Materials for Molecule Separation and Conversion*, ser. Micro and Nano Technologies, J. Liu and F. Ding, Eds. Elsevier, 2020, pp. 65–88. [Online]. Available: https://www.sciencedirect.com/science/article/pii/B9780128184875000030

[18] J. Bendoraitis, A. Chester, F. Dwyer, and W. Garwood, "Pore size and shape effects in zeolite catalysis," in *New Developments in Zeolite Science and Technology*, ser. Studies in Surface Science and Catalysis, Y. Murakami, A. Iijima, and J. Ward, Eds. Elsevier, 1986, vol. 28, pp. 669–675. [Online]. Available: https://www.sciencedirect.com/science/article/pii/S0167299109609332

[19] S. Narayanan, P. Tamizhdurai, V. L. Mangesh, C. Ragupathi, P. Santhana krishnan, and A. Ramesh, "Recent advances in the synthesis and applications of mordenite zeolite – review," *RSC Adv.*, vol. 11, pp. 250–267, 2021. [Online]. Available: http://dx.doi.org/10.1039/D0RA09434J

[20] A. N. van laak, R. W. Gosselink, S. L. Sagala, J. D. Meeldijk, P. E. de Jongh, and K. P. de Jong, "Alkaline treatment on commercially available aluminum rich mordenite," *Applied Catalysis A: General*, vol. 382, no. 1, pp. 65–72, 2010. [Online]. Available: https://www.sciencedirect.com/science/article/pii/S0926860X1000284X

[21] W. Lutz, "Zeolite y: Synthesis, modification, and properties—a case revisited," *Advances in Materials Science and Engineering*, vol. 2014, p. 724248, May 2014. [Online]. Available: https://doi.org/10.1155/2014/724248

[22] C. Sauer, G. J. L. de Reijer, A. Schaefer, and P.-A. Carlsson, "Isomorphous substitution of gallium into mfi-framework zeolite increases 2,5-dimethylfuran to aromatics selectivity and suppresses catalyst deactivation," *Topics in Catalysis*, Dec 2022. [Online]. Available: https://doi.org/10.1007/s11244-022-01776-2

[23] R. ling LIU, H. qing ZHU, Z. wei WU, Z. feng QIN, W. bin Fan, and J. guo WANG, "Aromatization of propane over ga-modified zsm-5 catalysts," *Journal of Fuel Chemistry and Technology*, vol. 43, no. 8, pp. 961–969, 2015. [Online]. Available: https://www.sciencedirect.com/science/article/pii/S187258131530027X

[24] Y. Zhou, H. Thirumalai, S. K. Smith, K. H. Whitmire, J. Liu, A. I. Frenkel, L. C. Grabow, and J. D. Rimer, "Ethylene dehydroaromatization over ga-zsm-5 catalysts: Nature and role of gallium speciation," *Angewandte Chemie International Edition*, vol. 59, no. 44, pp. 19 592–19 601. [Online]. Available: https://onlinelibrary.wiley.com/doi/abs/10.1002/anie.202007147

[25] J. Joly, H. Ajot, E. Merlen, F. Raatz, and F. Alario, "Parameters affecting the dispersion of the gallium phase of gallium h-mfi aromatization catalysts," *Applied Catalysis A: General*, vol. 79, no. 2, pp. 249–263, 1991. [Online]. Available: https://www.sciencedirect.com/science/article/pii/0926860X9180010V

[26] A. Al Ghatta and J. P. Hallett, "Bioderived furanic compounds as replacements for btx in chemical intermediate applications," *RSC Sustain.*, pp. –, 2023. [Online]. Available: http://dx.doi.org/10.1039/D3SU00038A

[27] D. D. Anggoro, H. Oktavianty, S. B. Sasongko, and L. Buchori, "Effect of dealumination on the acidity of zeolite y and the yield of glycerol mono stearate (gms)," *Chemosphere*, vol. 257, p. 127012, 2020. [Online]. Available: https://www.sciencedirect.com/science/article/pii/S0045653520312054

[28] E. A. Uslamin, B. Luna-Murillo, N. Kosinov, P. C. Bruijnincx, E. A. Pidko, B. M. Weckhuysen, and E. J. Hensen, "Gallium-promoted hzsm-5 zeolites as efficient catalysts for the aromatization of biomass-derived furans," *Chemical Engineering Science*, vol. 198, pp. 305–316, 2019. [Online]. Available: https://www.sciencedirect.com/science/article/pii/S0009250918306729

**DEPARTMENT OF CHEMICAL ENGINEERING**
**CHALMERS UNIVERSITY OF TECHNOLOGY**
Gothenburg, Sweden
www.chalmers.se


CHALMERS
UNIVERSITY OF TECHNOLOGY